Impacts of inductor nonlinear characteristic in multiconverter microgrids: Modeling, analysis, and mitigation

Yuan, Wenbin; Wang, Yanbo; Liu, Dong; Deng, Fujin; Chen, Zhe

Published in:
IEEE Journal of Emerging and Selected Topics in Power Electronics

DOI (link to publication from Publisher):
10.1109/JESTPE.2020.2970716

Publication date:
2020

Document Version
Accepted author manuscript, peer reviewed version

Impacts of Inductor Nonlinear Characteristic in Multiconverter Microgrids: Modeling, Analysis, and Mitigation

Wenbin Yuan, Yanbo Wang, *Senior Member, IEEE,* Dong Liu, *Senior Member, IEEE,* Fujin Deng, *Senior Member, IEEE,* Zhe Chen, *Fellow, IEEE*

***Abstract*—Powder magnetic materials are excellent alternative for filter inductor of power converter due to high saturation flux density and low cost. Unfortunately, inherent soft-saturation nonlinear characteristic of powder magnetic core can deteriorate control performance of power converter, which has been paid intensive attentions in individual grid-connected inverter. However, such impacts of nonlinear characteristic of filter inductors are merely concerned in multi-converter systems, where the control performance of paralleled converters is more complicated than that of individual converter. This paper investigates and mitigates impacts of nonlinear characteristic of filter inductor in multi-converter microgrids, so that the comprehensive performance can be improved in a cost-effective way. Average model of inductor is first established to quantitatively analyze the nonlinear characteristic. Then, impedance model of multi-converter microgrid is derived to analyze the effect of inductor nonlinear characteristic on power control performance. Furthermore, a robust droop control strategy is developed to mitigate the effect of inductor nonlinear characteristics on power control performance. In addition, sensitivity analysis is implemented to assess immunity capability of proposed control strategy on nonlinear inductor. Simulation and experimental results show that the proposed droop control strategy is able to perform desirable power control performance with a sound capability to mitigate the effect of nonlinear inductor, which thus improves operation performance and reduces design cost of multi-converter microgrid.**

***Keywords*—Nonlinear characteristic, filter inductor, multi-converter microgrid, powder core, robust droop control, nonlinear impedance compensation.**

I. INTRODUCTION

Power converters as important interfaces are indispensable components in modern energy system [1]-[2], which enables efficient conversion, generation and distribution of electrical energy [3], and improves reliability and resilience of power supply services [4]. In power converter, filter is commonly designed to attenuate switching ripple as an important component of power converter. In practical operation, various magnetic core materials such as powder core and ferrite core can be applied for filter design, which is highly related with operation performance and design cost of power converter. A comparative analysis for different magnetic materials is given in Table I by a comprehensive investigation from [5]-[14]. It can be seen that the advantages of powder magnetic material include high saturation flux density [5]-[11], low sensitivity to temperature variation and low cost [9]-[14]. Also, powder cores do not suffer from fringing loss or gap electromagnetic interference effect [8]-[10]. However, powder core inductor commonly exhibits nonlinear characteristic due to inherent soft-saturation nonlinearity of powder core [7]-[14], which can deteriorate control performance of power converter [8]-[9],[15]-[16]. On the other hand, the ferrite cores are widely applied due to good linear degree in linear region and low power loss during high-frequency range, but ferrite core has a higher cost than powder core and is sensitive to temperature variation [7],[10]. Compared with ferrite core, powder core is preferable option as filter inductor based on comprehensive performance indexes in practical application [7]-[14]. Fig. 1 shows the different operation characteristic of the two magnetic materials, which is explained as follows.

TABLE I
COMPARATIVE ANALYSIS FOR DIFFERENT MAGNETIC MATERIALS

	Application [5]-[6]	**Advantages** [7]-[14]	**Disadvantages** [7]-[14]
Powder Magnetic Cores	Filter inductor	➢ High saturation flux density ➢ Good robustness to temperature variation ➢ Small low-frequency loss ➢ Low cost	Soft-saturation nonlinearity
Ferrite Magnetic Cores	➢ Switched-mode power supply ➢ High-frequency transformer	➢ High linear Degree ➢ Small high-frequency loss	➢ High cost ➢ Sensitive to temperature variation ➢ Fringing loss

(1) ***Hard saturation characteristic*** [7],[10]: It means that the permeability of ferrite core does not vary with magnetic field strength in linear region. A sudden decrease of permeability would happen from nominal value to almost zero value as shown in red curve once

This work was supported by the ForsKEL and EUDP project "Voltage control and protection for a grid towards 100% power electronics and cable network (COPE)" (No. 880063).

Wenbin Yuan, Yanbo Wang, Dong Liu and Zhe Chen are with the Department of Energy Technology, Aalborg University, Aalborg 9220, Denmark (e-mail: wyu@et.aau.dk; ywa@et.aau.dk; dli@et.aau.dk; zch@et.aau.dk). (*Corresponding author: Yanbo Wang.*)

Fujin Deng is with the School of Electrical Engineering, Southeast University, Nanjing 210096, China (e-mail: fdeng@seu.edu.cn).

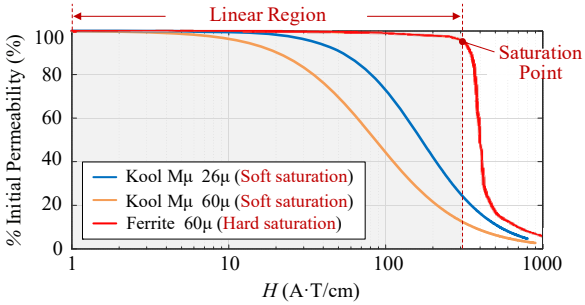

Fig. 1. Operation characteristic of different magnetic materials.

the inductor current is increased to saturation point. In practical design, power converter is operated in linear region by designing saturation point, where the permeability of inductor is almost constant.

(2) ***Soft-saturation characteristic*** [7]-[14]: It refers to an inherent nonlinear phenomenon, where permeability of powder core is slowly decreased as increase of inductor current as shown in blue and orange curves, which is an inherent drawback determined by powder magnetic material.

It can be seen from Fig. 1 that the powder core exhibits nonlinear characteristic during a wide current range, while ferrite core exhibits good linear degree as increase of output current (red curve) in linear region. In addition, different powder cores have different permeability-magnetic field strength relationships as shown in orange and blue curves (Kool Mμ 26μ and Kool Mμ 60μ).

In fact, operation characteristic of inductor is highly related with cost and design manufacture. The vision of this work is to compensate for the drawback of power core inductor (soft-saturation nonlinearity) by proposed control strategy, so that the ideal characteristic can be performed in a cost-effective way. The main contributions of this paper can be explained as follows. (1) Time-varying average model of inductor is established to investigate soft-saturation nonlinearity of filter inductor. (2) This work reveals how the inductor nonlinear characteristic affects control performance of paralleled converters by proposed impedance model. (3) A robust droop control strategy is proposed to mitigate the inherent drawback of inductor so that the comprehensive performance is improved in a cost-effective way. (4) Design guideline of controller is formulated to support practical application by proposed small signal stability, dynamic performance and sensitivity analysis.

The contributions of this work are promising in practical application, where the poor characteristic of inductor can be compensated by proposed control strategy. It means that the system performance is still satisfied even if poor-characteristic inductors are used, so that the system cost can be reduced. Note that the advantage of this work is more evident as increase of inverter number, where for a microgrid with n converters, the cost of inductors with number of $6\times n$ can be reduced as shown in Fig. 2.

The rest of this paper is organized as follows. In Section II, the effect of nonlinear inductor on power control performance in multi-converter microgrid is revealed by current-dependent output impedance modelling. In Section III, robust droop control strategy is proposed to mitigate the effect of nonlinear inductors. In addition, stability and sensitivity analysis are performed. In Section IV and V, simulation and experimental results are provided to validate effectiveness of the proposed robust droop control strategy. Conclusions are drawn in Section VI.

II. Problem Formulation and Proposed Analysis

In this section, the mechanism of problem is analyzed and the motivation of this work is explained. Then, the impact of nonlinear filter inductor in multi-converter microgrid is investigated.

A. Problem Formulation and Motivation

The effects of nonlinear characteristic of powder core inductor on control performance [8]-[9],[15]-[16] and closed-loop stability [16]-[17] of grid-connected inverter have been paid intensive attentions. The effect of nonlinear inductor on control performance of grid-connected PV inverter is originally investigated in [15], where a self-learning algorithm is adapted to calculate nonlinear inductance. A systematic *LCL* filter design method for grid-connected inverter considering nonlinear inductor is presented in [8], where the effect of nonlinear inductor on resonance phenomenon is analyzed. In [9], a compensation controller is presented to mitigate effect of nonlinear inductor on current quality in grid-connected converter. Considering soft-saturation nonlinearity of filter inductor, a direct digital control method of grid-connected inverter is proposed in [16], where a parameter space approach is developed to investigate system stability. A virtual impedance based stability analysis method is also developed in [17] to analyze stability of grid-connected inverters with nonlinear filter inductor. However, the aforementioned works mainly focus on the effect of nonlinear inductor in an individual inverter.

In fact, control performance of paralleled inverters is more complicated than individual inverter [18]-[23]. The complexity of power control performance may extend further once soft-saturation nonlinearity of filter inductor is considered, which is slightly concerned in previous works. To investigate effect of nonlinear inductor on control performance of paralleled converters and improve power control performance with immunity to nonlinear inductor, a robust droop control method is developed in this paper as an extension of our previous conference work [24]. The new contributions over [24] are explained as follows. (1) Stability, dynamic performance and sensitivity analysis are implemented to formulate design guideline of proposed controller and assess dynamic performance and nonlinearity-immunity capability of proposed control strategy. (2) The experimental results about soft-saturation nonlinearity of filter inductors are given to validate the practical nonlinearity phenomenon of filter inductors.

With increasing penetrations of renewable energy sources, multi-converter microgrid is becoming an attractive energy infrastructure that integrates various distributed generators (DGs), storage devices and local loads [25]-[27]. Fig. 2 shows circuit configuration of multi-converter microgrid, which can

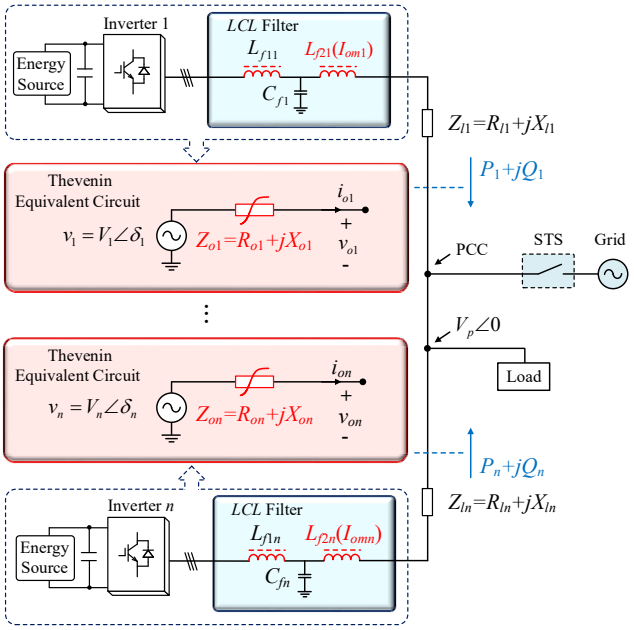

Fig. 2. The circuit configuration of *n*-converter microgrid.

be enabled in grid-connected mode and autonomous mode according to commands of power system. Filter is designed to attenuate the switching ripple of inverter. In this work, power control performance of multi-converter microgrid in autonomous mode is investigated with consideration of the effect of nonlinear filter inductor.

The classical *P-f* and *Q-V* power control strategy [28] is given as ~~(1)-(2).~~

$$\omega_i^* = \omega_0 - m_i P_i \tag{1}$$

$$V_i^* = V_0 - n_i Q_i \tag{2}$$

where ω_i^* *and* V_i^* are reference commands of angular frequency and output voltage amplitude. ω_0 and V_0 are angular frequency and output voltage amplitude of inverter without load. m_i and n_i are power rating-dependent droop coefficients of the *i*-th inverter.

The active power can be proportionally shared by conventional droop control strategy. The reactive power sharing performance is related with output impedance, feeder impedance and *Q-V* droop coefficient as (3) [19].

$$\frac{Q_1}{Q_2} = \frac{X_{o2}+X_{l2}+n_2V_p}{X_{o1}+X_{l1}+n_1V_p} \tag{3}$$

where X_{oi} is reactance of the equivalent output impedance of the *i*-th inverter. X_{li} is reactance of feeder impedance. V_p is voltage amplitude at the point of common coupling (PCC).

In practical operation, powder core is a preferred choice for power filter due to a high saturation level and low cost [5]-[14]. However, the inherent soft-saturation nonlinearity of inductor with powder core can lead to nonlinear output impedance of inverter, posing a challenge for reactive power sharing in multi-converter microgrid, which is merely addressed in previous work. Therefore, the effect of nonlinear inductor on power sharing performance is investigated in this section.

B. Proposed modelling and analysis on effect of nonlinear inductor on power control characteristic in droop-controlled microgrids

1) Nonlinear inductor modelling

~~In this section, the nonlinear inductor model is established to reveal soft-saturation nonlinearity of filter inductor.~~

The voltage u_L across an inductor can be given as (4) or (5).

$$u_L = L(i_L)\frac{di_L}{dt} \tag{4}$$

$$u_L = N\frac{d\Phi}{dt} \tag{5}$$

where L is current-dependent inductor. i_L is current through the inductor. N is turn number of coil and Φ is magnetic flux passing through the coil. Φ is defined as integration of magnetic flux density B over an area A, which is usually given as (6) with the assumption of constant B over A [29].

$$\Phi = BA \tag{6}$$

where B is given as (7).

$$B=\mu(H)H \tag{7}$$

where μ is magnetic permeability of inductor core. Magnetic permeability is a nonlinear function of magnetic field strength H, which is given as (8) according to characteristic of magnetic powder core [5].

$$\mu=\left(a+bH+cH^2+dH^3+eH^4\right)\cdot\mu_i \tag{8}$$

where μ_i is the initial permeability of powder core. a, b, c, d and e are coefficients of relationship between H and μ. Magnetic field strength H is given as (9) according to Ampere's circuital law [29].

$$H=\frac{Ni_L}{l} \tag{9}$$

where l is the length of a circle in toroid.

Magnetic permeability of powder core is obtained by combining (8) and (9) as (10), which is a nonlinear function of current i_L.

$$\mu'(i_L)=a'+b'i_L+c'i_L^2+d'i_L^3+e'i_L^4 \tag{10}$$

where

$$a'=a\mu_i,\ b'=\frac{b\mu_iN}{l},\ c'=\frac{c\mu_iN^2}{l^2},\ d'=\frac{d\mu_iN^3}{l^3},\ e'=\frac{e\mu_iN^4}{l^4}$$

Inductance of the inductor with magnetic powder core can be obtained by combining (4)-(10) as (11).

$$L(i_L)=N\frac{d\Phi}{di_L}=\frac{AN^2}{l}\left[\mu'(i_L)+i_L\frac{d\mu'(i_L)}{di_L}\right]=f(i_L) \tag{11}$$

Also, the average inductance can be defined for inductor current $i_L=I_m\sin(\omega t)$ as (12).

$$L_{avg}=\frac{1}{T}\int_0^T L(i_L)dt=a_{avg}+c_{avg}I_m^2+e_{avg}I_m^4=g(I_m) \tag{12}$$

where

$$a_{avg}=\frac{a\mu_i AN^2}{l},\ c_{avg}=\frac{3c\mu_i AN^4}{2l^3},\ e_{avg}=\frac{15e\mu_i AN^6}{8l^5}$$

In fact, the inductance used in previous work is an instantaneous value which is defined as (13).

$$L_{nom}=\lim_{i_L\to 0} L \tag{13}$$

Then, the current-dependent soft-saturation nonlinearity of inductor in (12) can be shown as Fig. 3 (taking L_{f21} and L_{f22} in Table II as an example). It can be seen that the actual inductances of powder core inductors can be changed as increase of load current, where the current-dependent inductance characteristics of two inductors are different due to difference of magnetic materials. The inherent nonlinear characteristic of powder magnetic core can also be seen in Fig. 1 according to datasheet [5]-[6], which shows that there exists nonlinearity of inductor with powder magnetic core and the permeability of inductor will converge to a small positive value as increase of magnetic field strength. Inductance will also converge to a small positive value according to the proposed inductor modelling as shown in Fig. 3, which can also be seen in the measured soft-saturation nonlinearity of filter inductors in Fig. 14. Note that the current through filter inductor is limited according to power rating of inverter in practical operation, which will limit the variation of filter inductor as shown in Fig. 3 and Fig. 14

The effect of soft-saturation nonlinearity on power control performance of droop-controlled microgrid is merely concerned in previous work, which will be systematically investigated in this work.

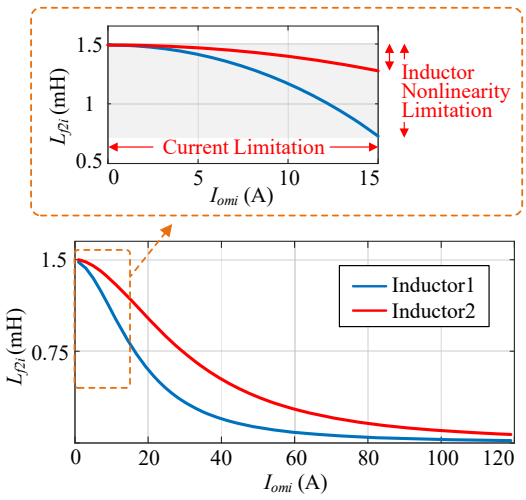

Fig. 3. Practical soft-saturation characteristics of inductors with different powder magnetic cores [30]-[31] as variation of load power.

2) Impedance modelling of multi-converter microgrid considering nonlinear inductor

In order to investigate the effect of nonlinear inductor on power control performance, closed-loop impedance model of multi-converter microgrid is derived considering nonlinear characteristic of filter inductor.

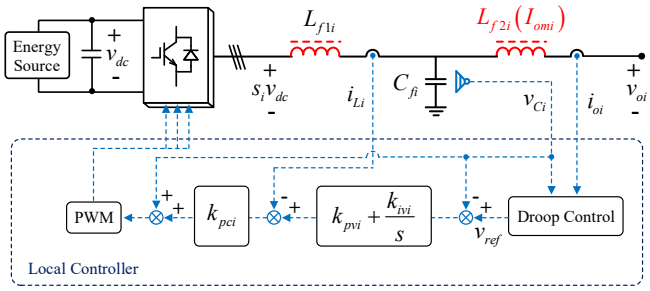

Fig. 4. The circuit configuration of inverter with local controller.

Fig. 4 shows the circuit configuration of inverter with local controller. Dynamic differential equations of this inverter can be given as (14).

$$\begin{cases} L_{f1i}\dfrac{di_{Li}}{dt}=s_i v_{dc}-v_{Ci} \\ C_{fi}\dfrac{dv_C}{dt}=i_{Li}-i_{oi} \\ L_{f2i}\dfrac{di_o}{dt}=v_{Ci}-v_{oi} \end{cases} \tag{14}$$

where s_i is control variable (1, 0 or -1), which depends on the state of switches. According to nonlinear control and feedback linearization theory [32]-[34], the open-loop averaged output-voltage dynamic can be derived as (15).

$$\begin{aligned} \langle s_i v_{dc}\rangle=&L_{f1i}C_{fi}\frac{d^2\langle v_{oi}\rangle}{dt}+\langle v_{oi}\rangle \\ &+L_{f1i}L_{f2i}C_{fi}\frac{d^3\langle i_{oi}\rangle}{dt}+L_{f1i}\frac{d\langle i_{oi}\rangle}{dt}+L_{f2i}\frac{d\langle i_{oi}\rangle}{dt} \end{aligned} \tag{15}$$

where $\langle\ \rangle$ means average value over one switching cycle.

For a voltage-controlled inverter, the outer voltage loop and inner current loop are adopted as shown in Fig. 4. The voltage controller is performed by PI controller with gains k_{pvi} and k_{ivi}, and current controller is performed by a proportional controller with gain k_{pci}. The dual-loop controller is given as (16).

$$\langle s_i v_{dc}\rangle=\langle v_{refi}\rangle+k_{pci}\begin{pmatrix} k_{pvi}\left(\langle v_{refi}\rangle-\langle v_{Ci}\rangle\right) \\ +k_{ivi}\int\left(\langle v_{refi}\rangle-\langle v_{Ci}\rangle\right)dt-\langle i_{Li}\rangle \end{pmatrix} \tag{16}$$

where v_{refi} is output voltage reference.

The output voltage of inverter can be given as (17) by combining (14)-(16).

$$V_{oi}(s)=G_i(s)V_{refi}(s)-Z_{oi}(s)I_{oi}(s) \tag{17}$$

where $G_i(s)$ is the voltage gain and $Z_{oi}(s)$ is output impedance, which are given as (19) and (20).

Substituting $s=j\omega_0$ into (20), the output impedance at fundamental frequency is obtained as (18).

$$X_{oi}(I_{omi})=\mathrm{Im}\left(Z_{oi}(I_{omi},s=j\omega_0)\right)=h\left(L_{f2i}(I_{omi})\right)=h'(I_{omi}) \tag{18}$$

$$G_i(s)=\frac{\left(1+k_{pci}k_{pvi}\right)s+k_{pci}k_{ivi}}{L_{f1i}C_{fi}s^3+k_{pci}C_{fi}s^2+\left(1+k_{pci}k_{pvi}\right)s+k_{pci}k_{ivi}} \tag{19}$$

$$Z_{oi}\left(I_{omi},s\right)=\frac{L_{f1i}L_{f2i}\left(I_{omi}\right)C_{fi}s^4+k_{pci}L_{f2i}\left(I_{omi}\right)C_{fi}s^3+\left(k_{pci}k_{pvi}L_{f2i}\left(I_{omi}\right)+L_{f1i}+L_{f2i}\left(I_{omi}\right)\right)s^2+\left(k_{pci}k_{ivi}L_{f2i}\left(I_{omi}\right)+k_{pci}\right)s}{L_{f1i}C_{fi}s^3+k_{pci}C_{fi}s^2+\left(1+k_{pci}k_{pvi}\right)s+k_{pci}k_{ivi}} \tag{20}$$

where I_{omi} is output current amplitude of i_{oi}. $L_{f2i}\left(I_{omi}\right)$ is the average inductance of filter inductor represented by model (12). It can be seen from (18) that the output impedance is related with the nonlinear inductor L_{f2i}, resulting in nonlinear and current-dependent characteristic of output impedance.

3) Analysis on effect of nonlinear inductor on reactive power control characteristic in droop-controlled microgrids

Considering nonlinear inductors, the ratio of output reactive power between two inverters is given as (21) by combining (3) and (18).

$$\frac{Q_1}{Q_2}=\frac{X_{o2}\left(I_{om2}\right)+X_{l2}+n_2V_p}{X_{o1}\left(I_{om1}\right)+X_{l1}+n_1V_p} \tag{21}$$

It can be seen from (3) and (21) that when nonlinearity of filter inductor is considered, reactive power sharing ratio becomes current-dependent and nonlinear. In order to investigate effect of nonlinear inductor on reactive power control characteristic, relationship between nonlinear inductor and reactive power sharing characteristic is shown in Fig. 5, based on a microgrid with two inverters and same feeder impedances. It can be seen from Fig. 5 that the soft-saturation nonlinearity of filter inductor causes nonlinear output impedance of inverter, which further deteriorates reactive power sharing performance. In addition, Fig. 5(c) shows that reactive power sharing ratio is time-varying as variation of load power when nonlinear inductor is considered. However, the existing droop control methods fail to deal with the effect of nonlinear inductor. Therefore, a robust droop control strategy is developed in Section III to improve accuracy of reactive power sharing with immunity to nonlinear inductor.

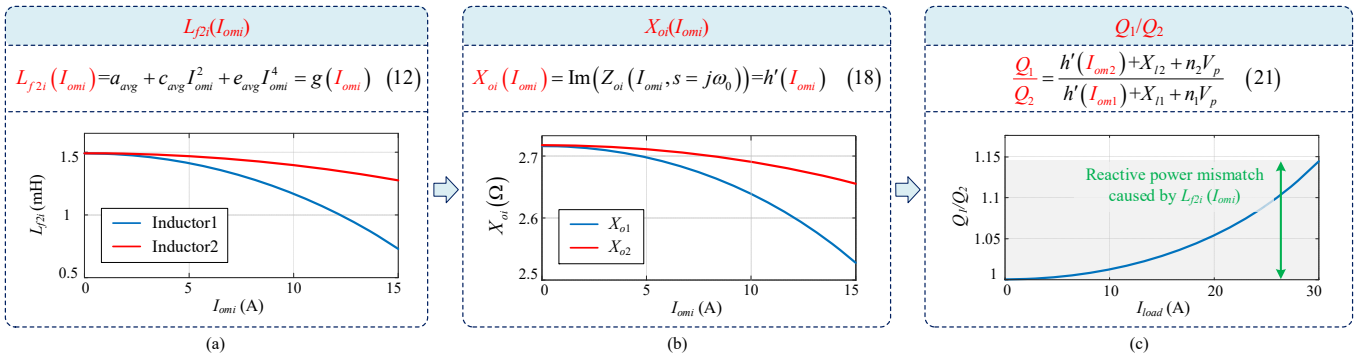

Fig. 5. Relationship between nonlinear inductor and reactive power sharing characteristic.

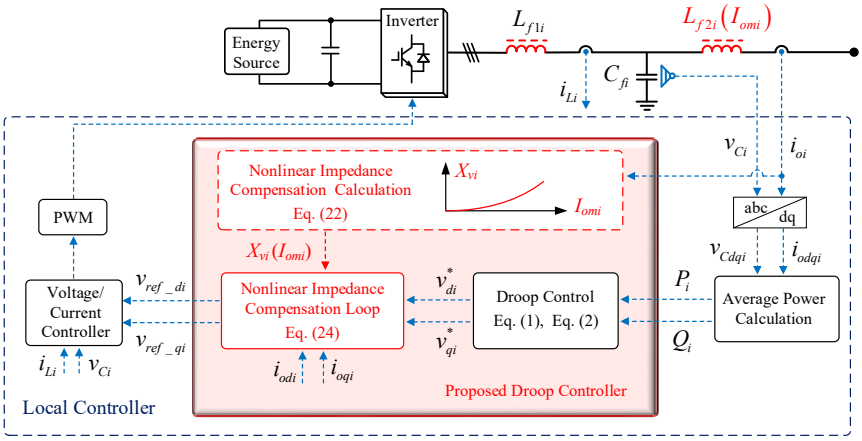

Fig. 6. The control diagram of proposed robust droop controller.

III. Proposed Robust Droop Control Against Nonlinear Inductor

To mitigate effect of nonlinear inductor on reactive power control performance, a robust droop control strategy is proposed, where nonlinear impedance compensation loop is developed to mitigate the effect of nonlinear inductor. In this work, a microgrid with two paralleled inverters is adopted to exemplify the proposed droop control strategy, where inductors with same nominal inductance but different soft-saturation characteristics are applied. The parameters are given in Table II.

A. Proposed robust droop control strategy

Fig. 6 shows control diagram of the proposed droop control strategy. In order to reject the effect of nonlinear inductor, a nonlinear impedance compensation loop is added to reshape output impedance of inverter. Instead of a static value, impedance compensation loop is adaptively tuned according to the established impedance model in Section II.B. Then, voltage reference obtained from droop controller is retuned by nonlinear impedance compensation loop, which is given as (22).

$$X_{vi}\left(I_{omi}\right)=X_{oi}^{*}-X_{oi}\left(I_{omi}\right) \tag{22}$$

where

$$X_{oi}^{*}=\frac{k}{Q_{\max i}} \tag{23}$$

where $X_{oi}(I_{omi})$ is current-dependent output impedance. X_{oi}^{*} is the equivalent fundamental impedance. k is a constant which is equal for all inverters.

Reference voltage incorporating nonlinear impedance compensation loop is given as (24).

$$\begin{cases} v_{ref\_di}=v_{di}^{*}+X_{vi}\left(I_{omi}\right)i_{oqi} \\ v_{ref\_qi}=v_{qi}^{*}-X_{vi}\left(I_{omi}\right)i_{odi} \end{cases} \tag{24}$$

where v_{di}^{*} and v_{qi}^{*} are original voltage references derived from droop control method, i_{odi} and i_{oqi} are inverter output current in dq frame. v_{ref_di} and v_{ref_qi} are updated voltage references in dq frame obtained from impedance compensation loop.

Fig. 7 shows Thevenin equivalent circuit of inverter with nonlinear impedance compensation loop. Then, the new reactive power sharing ratio of inverters with the proposed robust droop control strategy can be given as (25).

$$\frac{Q_1}{Q_2}=\frac{X_{o2}\left(I_{om2}\right)+X_{v2}\left(I_{om2}\right)+X_{l2}+n_2V_p}{X_{o1}\left(I_{om1}\right)+X_{v2}\left(I_{om1}\right)+X_{l1}+n_1V_p}=\frac{X_{o2}^{*}+X_{l2}+n_2V_p}{X_{o1}^{*}+X_{l1}+n_1V_p} \tag{25}$$

where X_{oi}^{*} is equivalent fundamental impedance which is the series impedance of $X_{oi}(I_{omi})$ and $X_{vi}(I_{omi})$.

By tuning the coefficient k in (23), $X_{oi}^{*}\gg(X_{li}+n_iV_p)$ can be ensured. Then, reactive power sharing is mainly determined by X_{oi}^{*} as (26), so that proportional reactive power sharing can be performed.

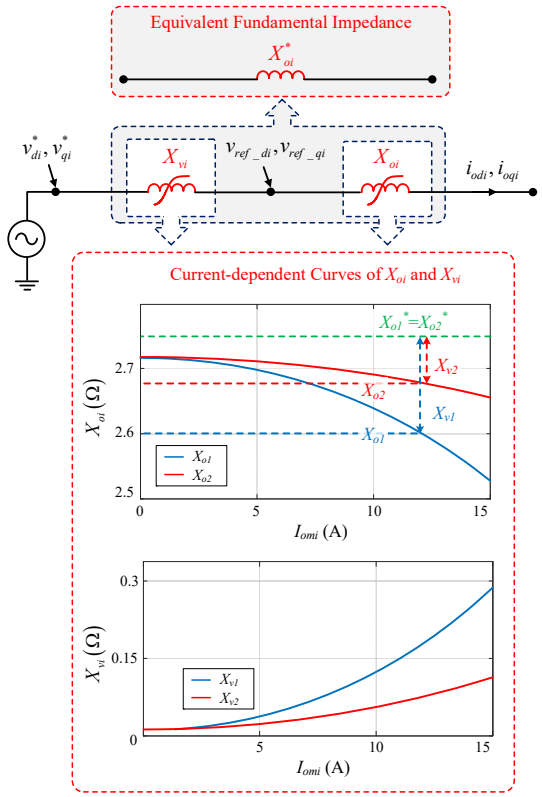

Fig. 7. Thevenin equivalent circuit of inverter with nonlinear impedance compensation loop.

$$\frac{Q_1}{Q_2}\approx\frac{X_{o2}^{*}}{X_{o1}^{*}}=\frac{Q_{\max 1}}{Q_{\max 2}} \tag{26}$$

B. Small signal modeling of the proposed robust droop control strategy

In this section, small signal model of multi-converter microgrids with proposed robust droop control strategy is first established considering nonlinear inductor.

With the proposed robust droop controller, voltage equation of filter capacitor can be given as (27).

$$\begin{cases} v_{Cdi}=v_{ref\_di}=V_0-n_iQ_i+X_{vi}\left(I_{omi}\right)i_{oqi} \\ v_{Cqi}=v_{ref\_qi}=0-X_{vi}\left(I_{omi}\right)i_{odi} \end{cases} \tag{27}$$

where

$$I_{omi}=\frac{\sqrt{P_i^2+Q_i^2}}{P_i}i_{odi} \tag{28}$$

Then, small signal equation of capacitor voltage can be obtained as (29) by linearizing (27).

$$\begin{bmatrix}\Delta v_{Cdi}\\ \Delta v_{Cqi}\end{bmatrix}=A_{1Vi}\begin{bmatrix}\Delta\delta_i\\ \Delta P_i\\ \Delta Q_i\end{bmatrix}+A_{2Vi}\begin{bmatrix}\Delta i_{odi}\\ \Delta i_{oqi}\end{bmatrix} \tag{29}$$

where A_{1Vi} and A_{2Vi} are parameter matrices that are given in Appendix.

Considering nonlinearity of filter inductor, the state equation of filter inductor is given as (30).

$$\begin{cases} \dot{i}_{odi} = \omega_i i_{oqi} + \dfrac{1}{L_{f2i}(I_{omi})} v_{Cdi} - \dfrac{1}{L_{f2i}(I_{omi})} v_{odi} \\ \dot{i}_{oqi} = -\omega_i i_{odi} + \dfrac{1}{L_{f2i}(I_{omi})} v_{Cqi} - \dfrac{1}{L_{f2i}(I_{omi})} v_{oqi} \end{cases} \tag{30}$$

Then, small signal dynamic equation of filter inductor can be derived as (31) by linearizing (30).

$$\begin{bmatrix} \Delta\dot{i}_{odi} \\ \Delta\dot{i}_{oqi} \end{bmatrix} = A_{1Ci} \begin{bmatrix} \Delta\delta_i \\ \Delta P_i \\ \Delta Q_i \end{bmatrix} + A_{2Ci} \begin{bmatrix} \Delta i_{odqi} \end{bmatrix} + B_{1Ci} \begin{bmatrix} \Delta v_{odi} \\ \Delta v_{oqi} \end{bmatrix} \tag{31}$$

where A_{1Ci}, A_{2Ci} and B_{1Ci} are given in Appendix.

Details of network and load models can be found in [35]-[37]. On the basis of this, small signal dynamics of the proposed power controller, nonlinear filter inductor, network and load can be represented in common DQ frame as (32)-(33).

$$\Delta\dot{x} = A\Delta x + B\Delta i_{disDQ} \tag{32}$$

$$\Delta y = C\Delta x + D\Delta i_{disDQ} \tag{33}$$

where Δx is the vector of state variables of the system and Δy is the vector of output variables of the system, which are shown in (34). Δi_{disDQ} is the unmeasured load disturbance. Details of parameter matrixes (A, B, C and D) are given in Appendix.

$$\begin{cases} \Delta x = \begin{bmatrix} \Delta x_{inv1} & \Delta x_{inv2} & \ldots & \Delta x_{invN} & \Delta i_{lineDQi} & \Delta i_{loadDQi} \end{bmatrix}^T \\ \Delta x_{invi} = \begin{bmatrix} \Delta\delta_i & \Delta P_i & \Delta Q_i & \Delta i_{odqi} \end{bmatrix}^T \\ \Delta y = \begin{bmatrix} \Delta x & \Delta Q_{i\_j} \end{bmatrix}^T \end{cases} \tag{34}$$

where Q_{i_j} is defined as (35) to indicate the reactive sharing error between inverter#i and inverter#j.

$$Q_{i\_j} = Q_i - Q_j \tag{35}$$

C. Stability, Dynamic Performance and Sensitivity analysis

In this section, stability, dynamic performance and sensitivity analysis are implemented based on the proposed small signal model.

Small signal stability of multi-converter microgrid with the proposed robust droop control is analyzed by eigenvalues of state matrix A. Fig. 8 shows dominant poles as variation of parameter k. It can be seen that λ_3 moves toward right half-plane as increase of k, where the critical value of stability region is 2.3e4. Meanwhile, λ_4-λ_5 move toward to imaginary axis as increase of k. Then, the damping ratio of system is decreased. Fig. 8 shows that k has critical influence on system stability and dynamic performance. Considering voltage droop limitation (less than 5%) and system dynamic performance, the stability region of k is given as $k\epsilon$[2.3e4, 5.5e4].

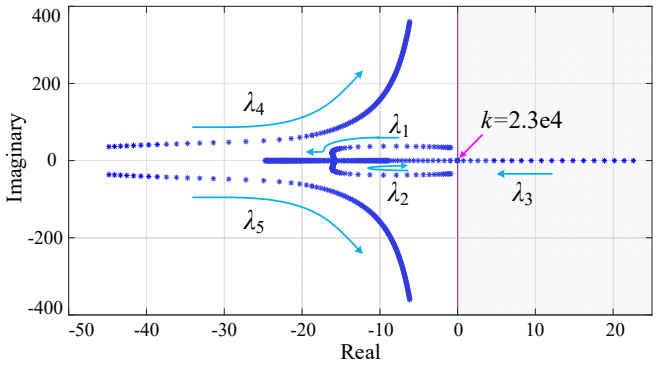

Fig. 8. Dominant poles as $k\epsilon$[2.2e4, 6e4].

Dynamic performance analysis is implemented to investigate dynamics of proposed controller over conventional droop controller. In fact, the system dynamic mainly depends on damping ratio which is defined as (36) [38].

$$\zeta = \frac{-\sigma}{\sqrt{\sigma^2 + \omega^2}} \tag{36}$$

where σ is the real part of eigenvalue and ω is the imaginary part of eigenvalue. Then, Fig. 9 shows dominant poles under conventional droop control strategy and proposed droop control strategy based on the same parameters as shown in Table II. It can be seen from Fig. 9 that system dynamic mainly depends on dominant poles λ_4-λ_5 [36],[38]. It can also be seen that damping ratio under proposed droop controller (ζ_{pro}=0.038) is bigger than that under conventional droop controller (ζ_{con}=0.009), which means that system dynamic under proposed droop controller is better than that under conventional droop controller.

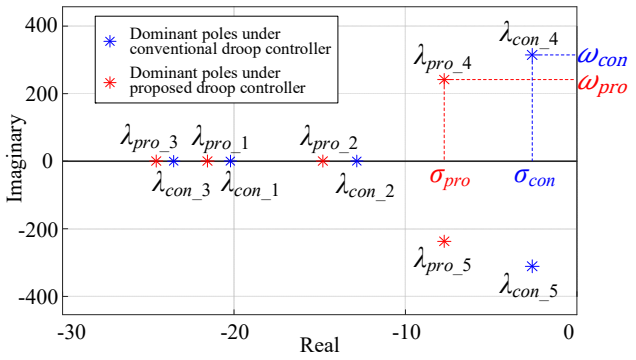

Fig. 9. Dominant poles under conventional droop control strategy and proposed droop control strategy with the same parameters.

Sensitivity analysis can provide clear insights into relationship among system states, inputs and outputs. To further theoretically investigate the effect of nonlinear characteristic of filter inductor on power control performance in multi-converter microgrid, sensitivity analysis is implemented to assess the immunity capability of proposed control strategy on nonlinear inductor.

In general, a dynamic system can be represented as (37)-(38).

$$\dot{x} = f(x, y, u) \quad x(t_0) = x_0 \tag{37}$$

$$0 = g(x, y, u) \quad y(t_0) = y_0 \tag{38}$$

where x, u and y are vectors of state variables, input variables, and system outputs. x_0, u_0 and y_0 are their initial values. The trajectory of system can be obtained as (39)-(40) by first-order linearization method [20].

$$x(t,x_0,u)=x(t,x_0,u_0)+x_u(t)(u-u_0) \tag{39}$$

$$y(t,x_0,u)=y(t,x_0,u_0)+y_u(t)(u-u_0) \tag{40}$$

where $x_u(t)$ and $y_u(t)$ are the sensitivity of $x(t)$ and $y(t)$ for control inputs. Then, changes of $x(t)$ and $y(t)$ with respect to the control inputs along with the system trajectory can be represented as (41)-(42).

$$\dot{x}_u=\frac{\partial f}{\partial x}x_u(t)+\frac{\partial f}{\partial y}y_u(t)+\frac{\partial f}{\partial u} \tag{41}$$

$$0=\frac{\partial g}{\partial x}x_u(t)+\frac{\partial g}{\partial y}y_u(t)+\frac{\partial g}{\partial u} \tag{42}$$

Fig. 10 shows sensitivity analysis results of reactive power sharing error Q_{1_2} under conventional droop control strategy and the proposed robust droop control strategy. The blue curve shows the sensitivity of Q_{1_2} under conventional droop control strategy without considering nonlinear characteristic of filter inductor. And the red one depicts sensitivity of reactive power sharing error Q_{1_2} under conventional droop control strategy considering nonlinear inductor. It can be seen from blue curve that the reactive power sharing is insensitive to current variation if nonlinear characteristic of filter inductor is neglected. If nonlinear characteristic of filter inductor is considered, the reactive power sharing error will increase 5Var for 1A current increment of load current. The green curve depicts the sensitivity of Q_{1_2} under proposed robust droop control strategy with nonlinear filter inductors, which shows that reactive power sharing error only increases 0.019Var for 1A current increment of load current.

The sensitivity results show that the accuracy of reactive power sharing can be deteriorated due to soft-saturation nonlinearity of filter inductor. However, the proposed robust droop control strategy can perform accurate reactive power sharing with immunity to nonlinear inductors.

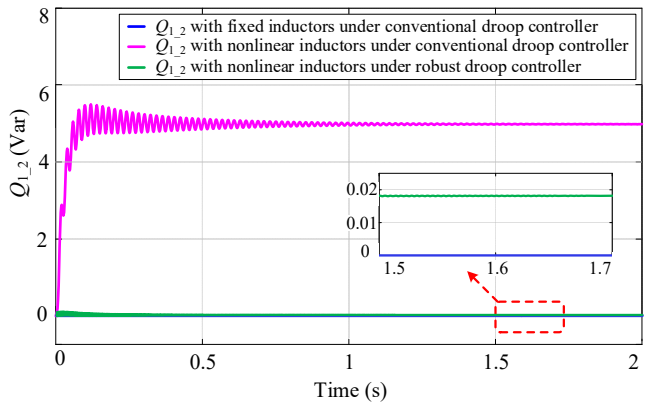

Fig. 10. Sensitivity analysis results for reactive power sharing control.

IV. Simulation Verification

To validate effectiveness of the proposed robust droop control strategy, simulation verification is implemented in a scale-down AC microgrid with two inverters in MATLAB/SIMULINK. Circuit configuration of the exemplified microgrid is shown in Fig. 2. The circuit and control parameters applied in simulation verification are given in Table II. Filter inductors with different soft-saturation characteristics are used, whose parameters can be seen in datasheets [30] and [31].

TABLE II
System Parameters Applied in Simulation

Filter Inductor Parameters			
	L_{f11}=L_{f21} [30]		L_{f12}=L_{f22} [31]
Manufacturer	MAGNETICS		MAGNETICS
Part number	Kool Mμ 00K6527E026		Kool Mμ 00K160LE026
Initial permeability	26μ		26μ
Nominal inductance	L_{f21_nom}=1.5mH		L_{f22_nom}=1.5mH
Circuit Parameters			
DC voltage	500V	Line impedance	Z_{l1}=(0.01+j0.31) Ω
Filter parameters	C_{f1}=C_{f2}=25μF		Z_{l2}=(0.01+j0.31) Ω
Control Parameters			
Droop coefficients	Case I	m_1= m_2=6e-5, n_1= n_2=6e-4	
	Case II	m_1= 6e-5, m_2= 1.2e-4, n_1=6e-4, n_2=1.2e-3	
Impedance compensation coefficient		k=3.5e4	
Switching frequency		f_{sw1}=f_{sw2} =10kHz	

Case I: Inverters with same power rating

In this case, the proposed droop control strategy is validated for paralleled inverters with same power rating, where time-varying load is exerted as 40% system capacity during 0-0.6s, 60% system capacity during 0.6-1.2s, 80% system capacity during 1.2-1.8s. Fig. 11(a)-(b) show active and reactive power sharing characteristic under conventional droop control strategy. It can be seen that active power of inverters can be equally shared. However, the accuracy of reactive power sharing is deteriorated due to the effect of nonlinear filter inductor as increase of load power, as shown in Fig. 11(b). Also, the reactive power distribution is time-varying as variation of load profiles, which agrees with theoretical analysis in Section II.B. Fig. 11(c)-(d) show active and reactive power sharing results under proposed droop control strategy. And Fig. 11(e) shows the nonlinear impedance compensation values under various load profiles. It can be seen that the impedance compensation values are adaptively tuned to deal with the effect of nonlinear inductors. Once the proposed droop control strategy is activated, the reactive power sharing error

can be eliminated and equal reactive power sharing can be implemented. It can also be seen from Fig. 11 that system dynamic under proposed droop control method is better than that under conventional droop control method. The simulation results agree with theoretical analysis in Section III.

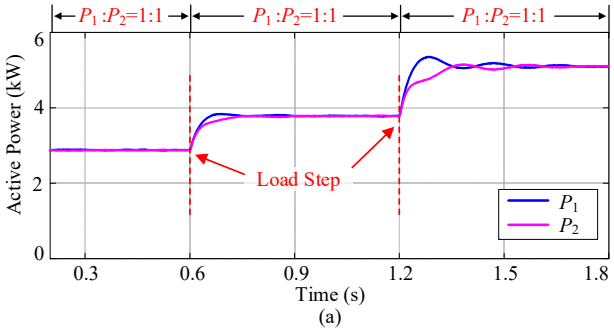

(a)

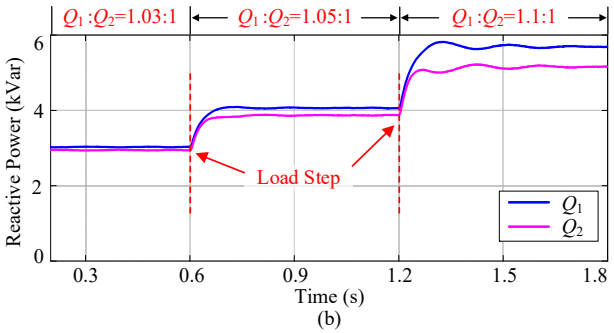

(b)

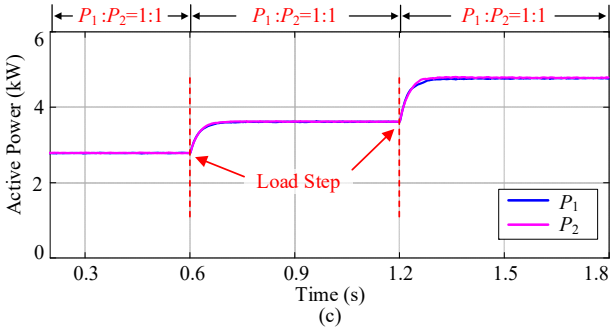

(c)

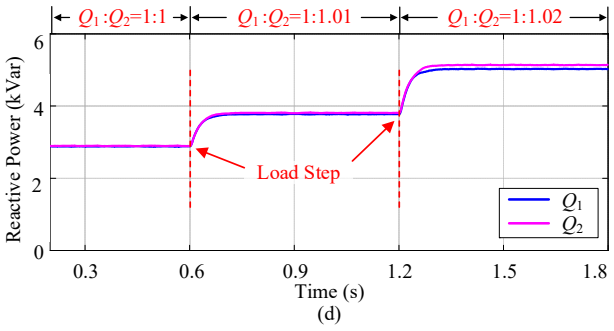

(d)

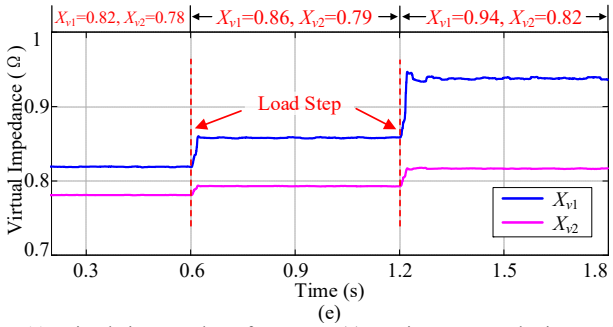

(e)

Fig. 11. Simulation results of case I. (a) Active power sharing under conventional droop control strategy. (b) Reactive power sharing under conventional droop control strategy. (c) Active power sharing under proposed droop control strategy. (d) Reactive power sharing under proposed droop control strategy. (e) Nonlinear impedance compensation values.

Case II: Inverters with different power ratings

Fig. 12 shows simulation results of paralleled inverters with different power ratings (S_{max1}:S_{max2}=2:1). Time-varying load is exerted as 40% system capacity during 0-0.6s, 60% system capacity during 0.6-1.2s, 80% system capacity during 1.2-1.8s. Fig. 12(a)-(b) show power sharing results under conventional droop control method. It can be seen that the reactive power sharing performance is deteriorated under conventional droop control strategy due to nonlinear inductors. Fig. 12(c)-(d) show active and reactive power sharing performance under proposed droop controller. Fig. 12(e) shows that the impedance compensation values are dynamically tuned to deal with the effect of nonlinear inductors. Also, it can be seen that dynamic performance of system is improved under the proposed droop control strategy. Therefore, the proposed method is able to implement proportional active and reactive power sharing and improve system dynamic with immunity to the effect of nonlinear inductor.

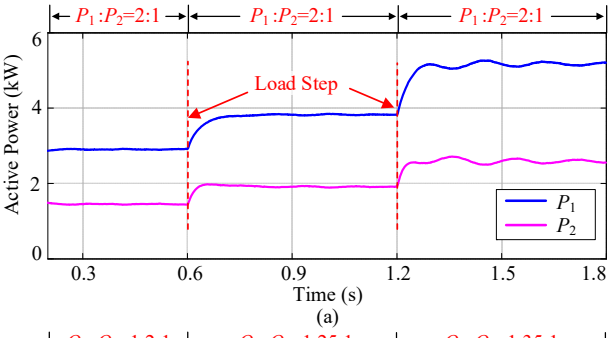

(a)

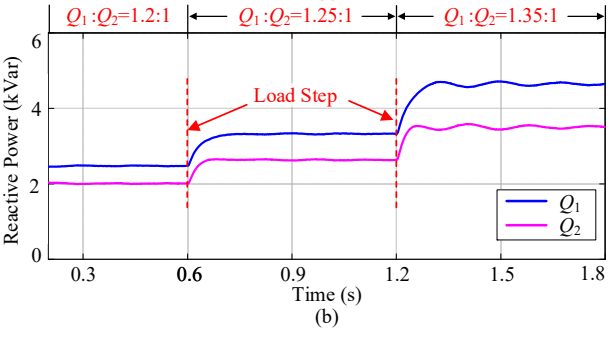

(b)

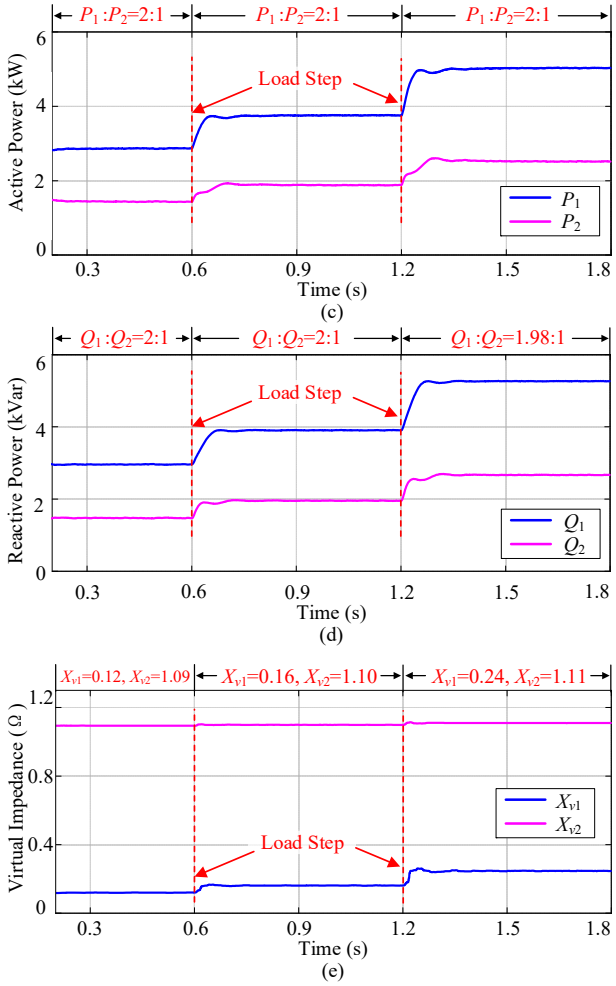

Fig. 12. Simulation results of case II. (a) Active power sharing under conventional droop control strategy. (b) Reactive power sharing under conventional droop control strategy. (c) Active power sharing under proposed droop control strategy. (d) Reactive power sharing under proposed droop control strategy. (e) Nonlinear impedance compensation values.

V. Experiment Verification

To further validate effectiveness of the proposed droop control strategy, experimental verification is implemented in a scaled-down microgrid with two inverters. The circuit diagram of exemplified microgrid is shown in Fig. 2. Fig. 13 shows a scale-down microgrid prototype which consists of paralleled voltage source converters, *LCL* filters, sampling circuit and DC source. The circuit and control parameters are given in Table III. The whole platform is controlled by dSPACE 1006. Inductors with same nominal inductance (0.8mH) and different magnetic powder cores are used as filter inductors. The practical inductor characteristic is measured by Precision Magnetics Analyzer 3260B made by Wayne Kerr Electronics. Fig. 14 shows the practical measured nonlinear characteristics of filter inductors as increase of bias current. It can be seen that the inductance of inductor in inverter1 has a poor characteristic as increase of bias current from 0A to 10A, while the inductance of inductor in inverter2 exhibits no obvious variation within the current range from 0A to 10A.

TABLE III
System Parameters Applied in Experiment

Circuit Parameters			
DC voltage	200V		
Filter parameters	C_{f1}=C_{f2}=25μF	Line impedance	Z_{l1}=(0.01+j0.56) Ω Z_{l2}=(0.01+j0.56) Ω
Control Parameters			
Droop coefficients	m_1= m_2=6e-5, n_1= n_2=6e-4		
Impedance compensation coefficient	k=3.5e4		
Switching frequency	f_{sw1}= f_{sw2} =10kHz		

Fig. 15 shows experimental results about output currents (Phase A) of paralleled inverters under conventional droop control strategy. It can be seen that the accuracy of reactive power sharing is deteriorated due to the effect of nonlinear filter inductor as variation of load power, which agrees with theoretical analysis in Section II.B.

Fig. 16 shows experimental results about output currents (Phase A) of paralleled inverters under the proposed droop control strategy. Experimental results show that the proposed robust droop control strategy can deal with nonlinear soft-saturation characteristic of filter inductor and perform accurate reactive power sharing within a wide load profile.

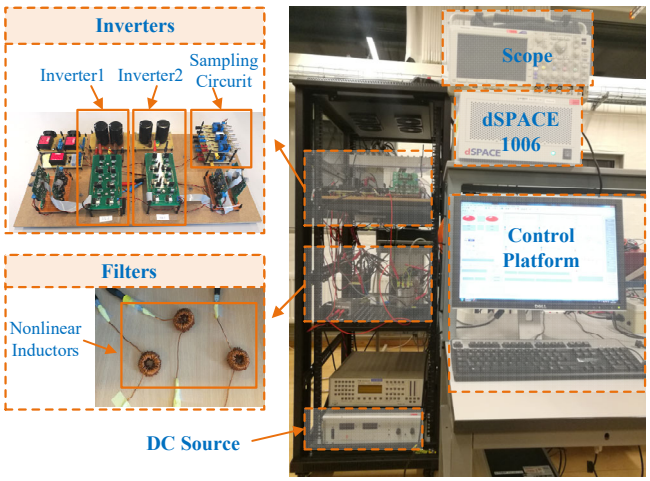

Fig. 13. Photo of experimental setup.

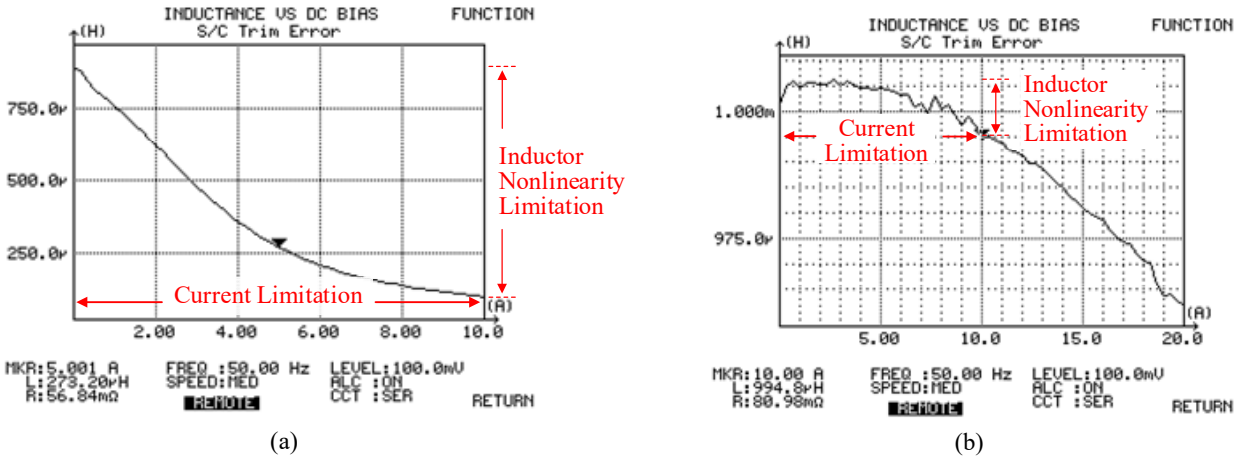

Fig. 14. Practical measured soft-saturation nonlinearity of filter inductors of two inverters. (a) Nonlinear characteristic of L_{f21}. (b) Nonlinear characteristic of L_{f22}.

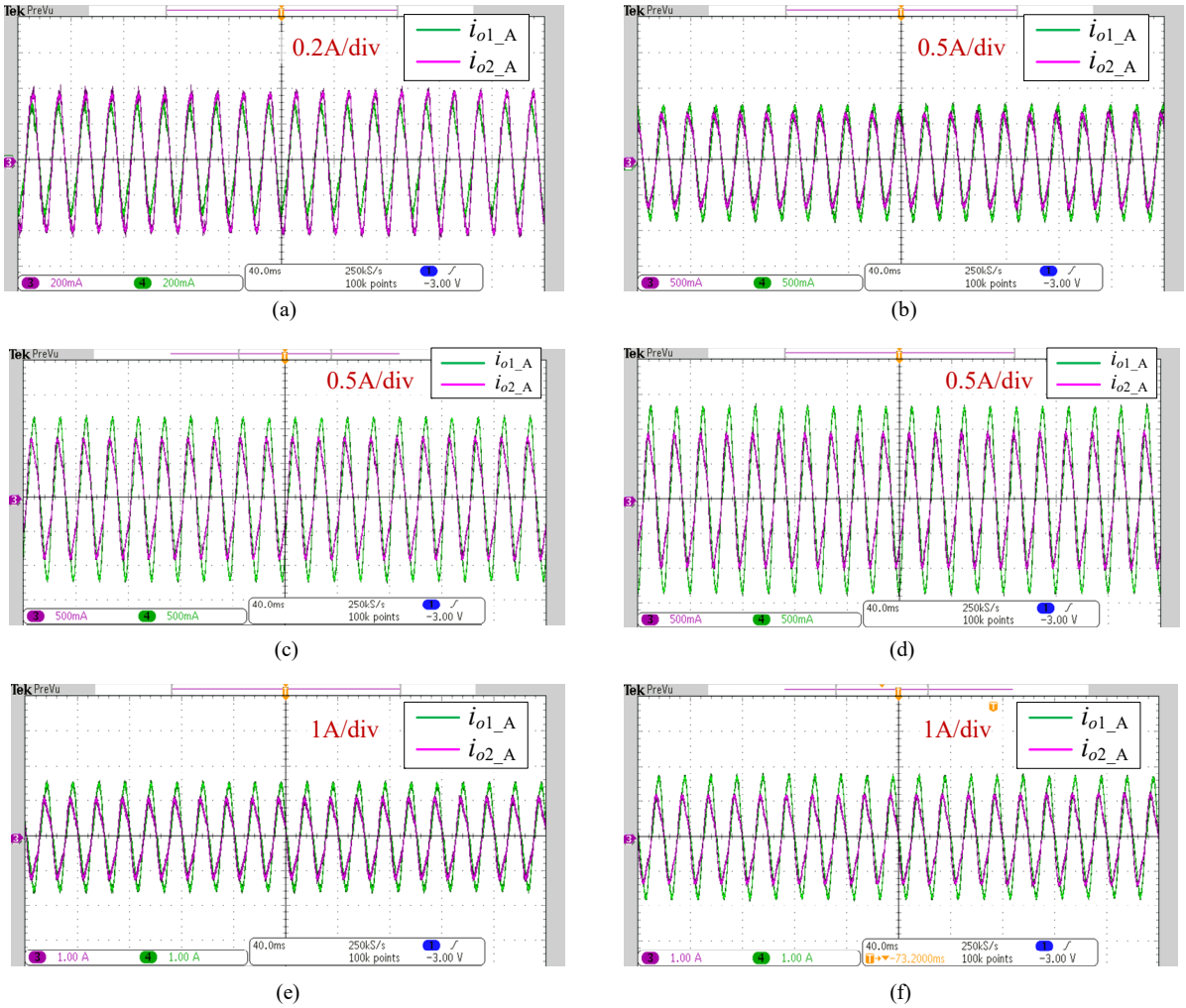

Fig. 15. Experimental results under conventional droop control strategy. (a) Output currents (Phase A) of paralleled inverters when current reference is 0.38A. (b) Output currents (Phase A) of paralleled inverters when current reference is 0.7A. (c) Output currents (Phase A) of paralleled inverters when current reference is 1A. (d) Output currents (Phase A) of paralleled inverters when current reference is 1.1A. (e) Output currents (Phase A) of paralleled inverters when current reference is 1.25A. (f) Output currents (Phase A) of paralleled inverters when current reference is 1.5A.

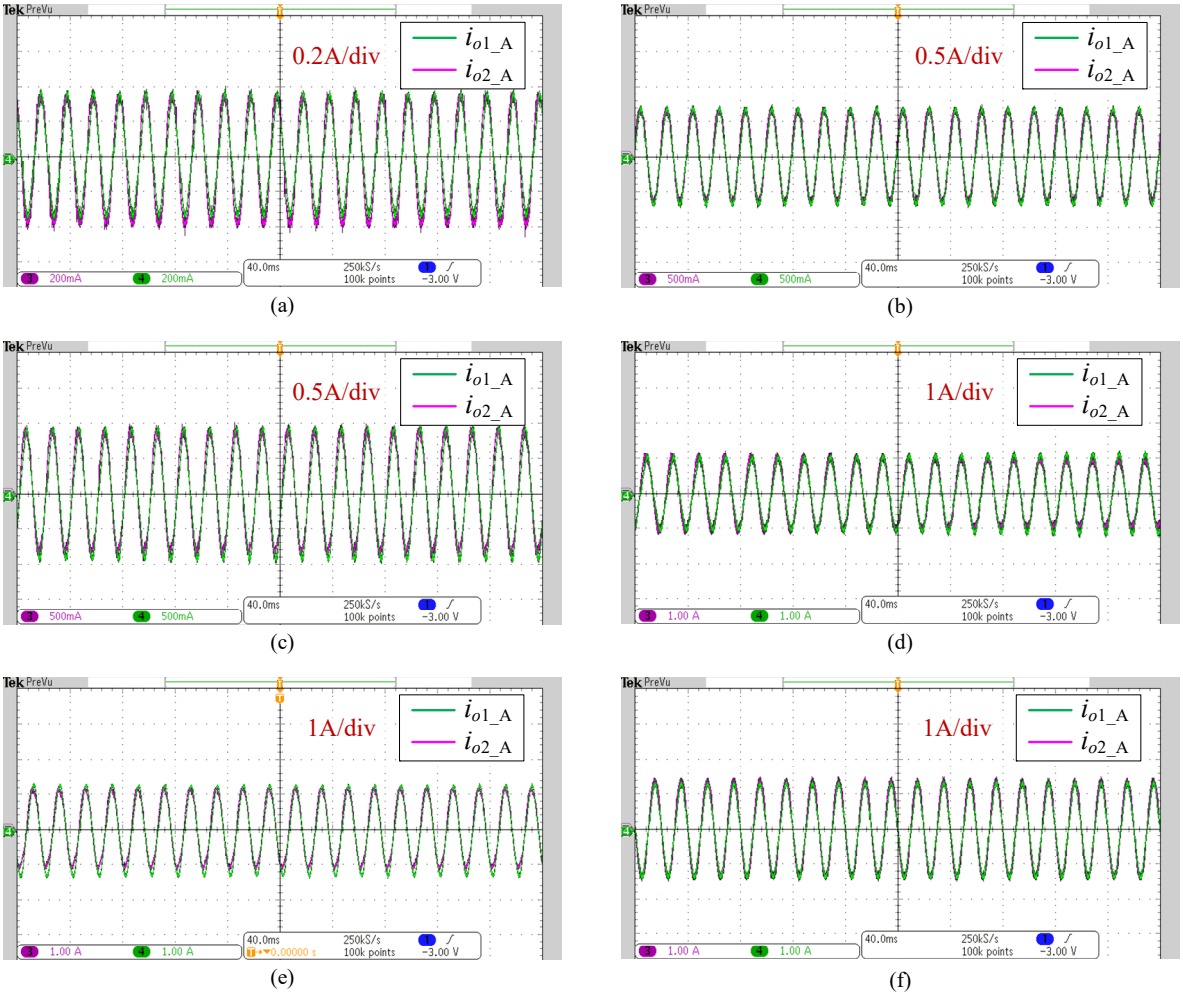

Fig. 16. Experimental results under the proposed robust droop control strategy. (a) Output currents (Phase A) of paralleled inverters when current reference is 0.38A. (b) Output currents (Phase A) of paralleled inverters when current reference is 0.7A. (c) Output currents (Phase A) of paralleled inverters when current reference is 1A. (d) Output currents (Phase A) of paralleled inverters when current reference is 1.1A. (e) Output currents (Phase A) of paralleled inverters when current reference is 1.25A. (f) Output currents (Phase A) of paralleled inverters when current reference is 1.5A.

VI. Conclusion

The inherent nonlinear characteristic of powder core inductor can deteriorate control performance of power converter. The aim of this work is to compensate the drawback by proposed control strategy so that the optimal comprehensive performance of filter inductor can be achieved in a cost-effective way. This paper investigates and addresses the impacts of nonlinear characteristic of filter inductor on operation performance of multi-converter microgrids. The proposed impedance model shows that the nonlinear characteristic of powder magnetic inductor can deteriorate reactive power control performance in multi-converter microgrids. Small signal stability analysis shows the parameter of nonlinear impedance compensation loop has important influence on stability of the proposed droop control strategy. Dynamic performance analysis reveals that proposed control strategy can improve system transient behavior mitigating the effect of nonlinear inductors. And sensitivity analysis shows that proposed control strategy has a good immunity capability on nonlinear inductor. Simulation and experimental results show the proposed control strategy is able to perform desirable control performance with immunity to nonlinear inductor, so that the comprehensive performance of multi-converter microgrids can be improved in a cost-effective way. This work can contribute to practical inductor design in multi-converter microgrids with desirable power control performance but low design cost.

Appendix

Parameter matrices in (29) are given as (43).

$$\begin{cases} A_{1Vi}=\begin{bmatrix} 0 & -i_{oqi\_0}K_{X_{oi}\_P_i} & -n_i-i_{oqi\_0}K_{X_{oi}\_Q_i} \\ 0 & i_{odi\_0}K_{X_{oi}\_P_i} & i_{odi\_0}K_{X_{oi}\_Q_i} \end{bmatrix} \\ A_{2Vi}=\begin{bmatrix} -i_{oqi\_0}K_{X_{oi}\_i_{odi}} & \dfrac{k}{Q_{\max i}}-X_{oi\_0} \\ -\dfrac{k}{Q_{\max i}}+X_{oi\_0}+i_{odi\_0}K_{X_{oi}\_i_{odi}} & 0 \end{bmatrix} \end{cases} \tag{43}$$

where

$$\begin{cases} K_{X_{oi}\_P_i}=\left.\dfrac{\partial X_{oi}\left(I_{omi}\right)}{\partial P_i}\right|_{P_{i\_0},Q_{i\_0},i_{odi\_0}} \\ K_{X_{oi}\_Q_i}=\left.\dfrac{\partial X_{oi}\left(I_{omi}\right)}{\partial Q_i}\right|_{P_{i\_0},Q_{i\_0},i_{odi\_0}} \\ K_{X_{oi}\_i_{odi}}=\left.\dfrac{\partial X_{oi}\left(I_{omi}\right)}{\partial i_{odi}}\right|_{P_{i\_0},Q_{i\_0},i_{odi\_0}} \end{cases} \tag{44}$$

where P_{i_0}, Q_{i_0}, i_{odi_0} and i_{oqi_0} are stable state values of output active power, reactive power and current of the i-th inverter. X_{oi_0} is the output impedance under P_{i_0}, Q_{i_0} and i_{odi_0}.

Parameter matrixes in (31) are given as (45), where v_{Cdi_0}, v_{Cqi_0}, v_{odi_0} and v_{oqi_0} are stable state values of filter capacitor voltage and output voltage of the i-th inverter. L_{f2i_0} is the inductance of filter inductor under P_{i_0}, Q_{i_0} and i_{odi_0}.

Taking a microgrid with two paralleled inverters as an example, parameter matrixes in (32)-(33) are given as (46)–(47), where v_{pD_0} and v_{pQ_0} are stable state values of common bus voltage in common DQ frame [36]. δ_{i_frame} is the angle between the reference frame of i-th inverter and the common reference frame [36].

$$\begin{cases} A_{1Ci}=\begin{bmatrix} 0 & -m_i i_{oqi\_0}-\dfrac{i_{oqi\_0}K_{X_{oi}\_P_i}}{L_{f2i\_0}}+\dfrac{\left(v_{odi\_0}-v_{Cdi\_0}\right)K_{L_{f2i}\_P_i}}{L_{f2i\_0}^2} & \dfrac{-n_i-i_{oqi\_0}K_{X_{oi}\_Q_i}}{L_{f2i\_0}}+\dfrac{\left(v_{odi\_0}-v_{Cdi\_0}\right)K_{L_{f2i}\_Q_i}}{L_{f2i\_0}^2} \\ 0 & m_i i_{odi\_0}+\dfrac{i_{odi\_0}K_{X_{oi}\_P_i}}{L_{f2i\_0}}+\dfrac{\left(v_{oqi\_0}-v_{Cqi\_0}\right)K_{L_{f2i}\_P_i}}{L_{f2i\_0}^2} & i_{odi\_0}K_{X_{oi}\_Q_i}+\dfrac{\left(v_{oqi\_0}-v_{Cqi\_0}\right)K_{L_{f2i}\_Q_i}}{L_{f2i\_0}^2} \end{bmatrix} \\ A_{2Ci}=\begin{bmatrix} \dfrac{\left(-v_{Cdi\_0}+v_{odi\_0}\right)K_{L_{f2i}\_i_{odi}}}{L_{f2i\_0}^2}-\dfrac{i_{oqi\_0}K_{X_{oi}\_i_{odi}}}{L_{f2i\_0}} & \omega_{i\_0}+\dfrac{\left(\dfrac{k}{Q_{\max i}}-X_{oi\_0}\right)}{L_{f2i\_0}} \\ \dfrac{\left(-v_{Cqi\_0}+v_{oqi\_0}\right)K_{L_{f2i}\_i_{odi}}}{L_{f2i\_0}^2}-\omega_{i\_0}+\dfrac{\left(-\dfrac{k}{Q_{\max i}}+X_{oi\_0}+i_{odi\_0}K_{X_{oi}\_i_{odi}}\right)}{L_{f2i\_0}} & 0 \end{bmatrix} \\ B_{1Ci}=\begin{bmatrix} -\dfrac{1}{L_{f2i\_0}} & 0 \\ 0 & -\dfrac{1}{L_{f2i\_0}} \end{bmatrix} \end{cases} \tag{45}$$

$$\begin{cases} A=\begin{bmatrix} A_{INV}+B_{INV}M_{INV}C_{INVc} & B_{INV}M_{1line} & 0_{10\times 2} \\ B_{1line}M_{INV}C_{INVc}+B_{3line}C_{INV\omega} & A_{line}+B_{1line}M_{1line}+B_{2line}M_{2line} & B_{2line}M_{load} \\ B_{2load}C_{INV\omega} & B_{1load}M_{2line} & A_{load}+B_{1load}M_{load} \end{bmatrix} \\ B=\begin{bmatrix} 0_{10\times 2} \\ B_{2line}M_{dis} \\ B_{1load}M_{dis} \end{bmatrix},\ C=\begin{bmatrix} diag\left(\begin{bmatrix}1 & 1 & \cdots & 1\end{bmatrix}_{1\times 16}\right) \\ C_1 \end{bmatrix},\ D=[0]_{17\times 2} \end{cases} \tag{46}$$

$$
\begin{cases}
A_{INV} = A_{INV1} + B_{\omega com} C_{INV\omega} \\
where \\
A_{INV1} = \begin{bmatrix} A_{inv1} & 0_{5\times5} \\ 0_{5\times5} & A_{inv2} \end{bmatrix}, A_{invi} = \begin{bmatrix} A_{1Pi} & A_{2Pi} \\ A_{1Ci} + \begin{bmatrix} B_{1Ci} T_{Vi}^{-1} & 0_{2\times1} & 0_{2\times1} \end{bmatrix} & A_{2Ci} \end{bmatrix}, A_{1Pi} = \begin{bmatrix} 0 & -m_i & 0 \\ 0 & -\omega_c & -\omega_c n_i i_{odi\_0} \\ 0 & 0 & -\omega_c - \omega_c n_i i_{oqi\_0} \end{bmatrix}, \\
A_{2Pi} = \begin{bmatrix} 0 & 0 \\ -\dfrac{\omega_c i_{oqi\_0} k}{Q_{\max i}} + \omega_c i_{oqi\_0} X_{oi\_0} + \omega_c v_{Cdi\_0} & \dfrac{\omega_c i_{odi\_0} k}{Q_{\max i}} - \omega_c i_{odi\_0} X_{oi\_0} + \omega_c v_{Cqi\_0} \\ -\omega_c i_{odi\_0}^2 K_{X_{oi\_}i_{odi}} - \omega_c i_{oqi\_0}^2 K_{X_{oi\_}i_{odi}} - \omega_c i_{odi\_0} X_{oi\_0} + \dfrac{\omega_c i_{odi\_0} k}{Q_{\max i}} - \omega_c v_{Cqi\_0} & \dfrac{\omega_c i_{oqi\_0} k}{Q_{\max i}} - \omega_c i_{oqi\_0} X_{oi\_0} + \omega_c v_{Cdi\_0} \end{bmatrix} \\
T_{Vi}^{-1} = \begin{bmatrix} -v_{pD\_0} \sin\left(\delta_{i\_\text{frame}}\right) + v_{pQ\_0} \cos\left(\delta_{i\_\text{frame}}\right) \\ -v_{pD\_0} \cos\left(\delta_{i\_\text{frame}}\right) - v_{pQ\_0} \sin\left(\delta_{i\_\text{frame}}\right) \end{bmatrix} \\
B_{\omega com} = \begin{bmatrix} B_{\omega com1} \\ B_{\omega com2} \end{bmatrix}, B_{\omega comi} = \begin{bmatrix} -1 & 0_{1\times4} \end{bmatrix}^T \\
C_{INV\omega} = \begin{bmatrix} 0 & -m_1 & 0_{1\times8} \end{bmatrix}
\end{cases}
$$

$$
\begin{cases}
B_{INV} = \begin{bmatrix} B_{inv1} & 0_{5\times2} \\ 0_{5\times2} & B_{inv2} \end{bmatrix} \\
where \\
B_{invi} = \begin{bmatrix} 0_{3\times2} \\ B_{1Ci} T_{Si}^{-1} \end{bmatrix}, T_{Si} = \begin{bmatrix} \cos\left(\delta_{i\_\text{frame}}\right) & -\sin\left(\delta_{i\_\text{frame}}\right) \\ \sin\left(\delta_{i\_\text{frame}}\right) & \cos\left(\delta_{i\_\text{frame}}\right) \end{bmatrix}
\end{cases}
\quad
\begin{cases}
C_{INVc} = \begin{bmatrix} C_{invc1} & 0_{2\times5} \\ 0_{2\times5} & C_{invc2} \end{bmatrix} \\
where \\
C_{invci} = \begin{bmatrix} T_{Ci} & 0_{2*1} & 0_{2*1} & T_{Si} \end{bmatrix}, \\
T_{Ci} = \begin{bmatrix} -i_{odi\_0} \sin\left(\delta_{i\_\text{frame}}\right) - i_{oqi\_0} \cos\left(\delta_{i\_\text{frame}}\right) \\ i_{odi\_0} \cos\left(\delta_{i\_\text{frame}}\right) - i_{oqi\_0} \sin\left(\delta_{i\_\text{frame}}\right) \end{bmatrix}
\end{cases}
$$

$$
\begin{cases}
B_{1line} = \begin{bmatrix} B_{1line1} & 0_{2*2} \\ 0_{2*2} & B_{1line2} \end{bmatrix} \\
where \\
B_{1linei} = \begin{bmatrix} \dfrac{1}{L_{linei}} & 0 \\ 0 & \dfrac{1}{L_{linei}} \end{bmatrix}
\end{cases}
\quad
\begin{cases}
B_{2line} = \begin{bmatrix} B_{2line1} \\ B_{2line2} \end{bmatrix} \\
where \\
B_{2linei} = \begin{bmatrix} -\dfrac{1}{L_{linei}} & 0 \\ 0 & -\dfrac{1}{L_{linei}} \end{bmatrix}
\end{cases}
\quad
\begin{cases}
B_{3line} = \begin{bmatrix} B_{3line1} \\ B_{3line2} \end{bmatrix} \\
where \\
B_{3linei} = \begin{bmatrix} i_{lineQi\_0} \\ -i_{lineDi\_0} \end{bmatrix}
\end{cases}
\quad
\begin{cases}
B_{1load} = \begin{bmatrix} \dfrac{1}{L_{load}} & 0 \\ 0 & \dfrac{1}{L_{load}} \end{bmatrix} \\
B_{2load} = \begin{bmatrix} i_{loadQ\_0} \\ -i_{loadD\_0} \end{bmatrix}
\end{cases}
$$

$$
\begin{cases}
M_{INV} = \begin{bmatrix} R_N & 0 & 0 & 0 \\ 0 & R_N & 0 & 0 \\ 0 & 0 & R_N & 0 \\ 0 & 0 & 0 & R_N \end{bmatrix}, M_{1line} = -M_{INV}, M_{2line} = \begin{bmatrix} R_N & 0 & R_N & 0 \\ 0 & R_N & 0 & R_N \end{bmatrix}, M_{load} = \begin{bmatrix} -R_N & 0 \\ 0 & -R_N \end{bmatrix}, M_{dis} = M_{load}
\end{cases}
\tag{47}
$$

$$
\begin{cases}
C_1 = \begin{bmatrix} 0 & 0 & 1 & 0_{1\times4} & -1 & 0_{1\times8} \end{bmatrix}
\end{cases}
$$

REFERENCES

[1] Y. Leng, X. Ruan, Q. Jin, and Y. Wang, "Current control strategies for parallel-form switch-linear hybrid envelope tracking power supply with two switched-mode converters to achieve optimal power allocation," *IEEE J. Emerg. Sel. Topics Power Electron.*, vol. 7, no. 4, pp. 2356-2368, Dec. 2019.

[2] M. Huang, Y. Peng, C. K. Tse, Y. Liu, J. Sun, and X. Zha, "Bifurcation and large-signal stability analysis of three-phase voltage source converter under grid voltage dips," *IEEE Trans. Power Electron.*, vol. 32, no. 11, pp. 8868-8879, Nov. 2017.

[3] X. Li, X. Ruan, X. Xiong, Q. Jin, and C. K. Tse, "Stability issue of cascaded systems with consideration of switching ripple interaction," *IEEE Trans. Power Electron.*, vol. 34, no. 7, pp. 7040-7052, Jul. 2019.

[4] K. Hariharan and S. Kapat, "Near optimal controller tuning in a current-mode DPWM boost converter in CCM and application to a dimmable LED array driving," *IEEE J. Emerg. Sel. Topics Power Electron.*, vol. 7, no. 2, pp. 1031-1043, Jun. 2019.

[5] Powder Cores-Product Catalog of Magnetics. "Magnetics powder core catalog."

[6] Ferrite Cores-Product Catalog of Magnetics. "Magnetics ferrite core catalog."

[7] G. R. C. Mouli, J. Schijffelen, P. Bauer, and M. Zeman, "Estimation of ripple and inductance roll off when using powdered iron core inductors," in *Proc. PCIM Europe*, 2016, pp. 1-8.

[8] T. F. Wu, M. Misra, L. C. Lin, and C. W. Hsu, "An improved resonant frequency based systematic LCL filter design method for grid-connected inverter," *IEEE Trans. Ind. Electron.*, vol. 64, no. 8, pp. 6412-6421, Aug. 2017.

[9] Q. Wei, B. Liu, and S. Duan, "Current ripple analysis and controller design for grid-connected converters considering the soft-saturation nature of the powder cores," *IEEE Trans. Power Electron.*, vol. 33, no. 10, pp. 8827-8837, Oct. 2018.

[10] M. A. Swihart, "Inductor cores–material and shape choices," Magnetics, Pittsburgh, PA, USA, 2004. [Online]. Available: htts://www.mag-inc.com

[11] S. Jayalath, D. Ongayo, and M. Hanif, "Modelling powder core inductors for passive filters in inverters using finite element analysis," *Electronics Letters*, vol. 53, no. 3, pp. 179-181, Feb. 2017.

[12] Y. Liu, H. A. Mantooth, J. C. Balda, and C. Farnell, "Realization of high-current variable AC filter inductors using silicon iron powder magnetic core," In *Proc. IEEE APEC*, 2017, pp. 855-860.

[13] Y. Liu, H. A. Mantooth, J. C. Balda, and C. Farnell, "A variable inductor based LCL filter for large-scale microgrid application," *IEEE Trans. Power Electron.*, vol. 33, no. 9, pp. 7338-7348, Sep. 2018.

[14] H. Gurleyen, E. Mese, J. H. Kim, and B. Sarlioglu, "Nonlinear analytical model of an inductance considering saturation and temperature variation," In *Proc. IEEE ECCE*, 2017, pp. 3150-3154.

[15] T. F. Wu, H. S. Nien, C. L. Shen, and T. M. Chen, "A single-phase inverter system for PV power injection and active power filtering with nonlinear inductor consideration," *IEEE Trans. Ind. Appl.*, vol. 41, no. 4, pp. 1075-1083, Jul./Aug. 2005.

[16] T. F. Wu, M. Misra, Y. Y. Jhang, Y. H. Huang, and L. C. Lin, "Direct digital control of single-phase grid-connected inverters with LCL filter based on inductance estimation model," *IEEE Trans. Power Electron.*, vol. 34, no. 2, pp. 1851-1862, Feb. 2019.

[17] T. F. Wu, M. Misra, Y. Y. Jhang, and C. Y. Lin, "Virtual impedance based stability analysis for direct digital controlled single-phase grid-connected inverter with LCL filter having wide inductance variation," *in Proc. APEC*, 2018, pp. 963-968.

[18] W. Yuan, Y. Wang, D. Liu, F. Deng, and Z. Chen, "Efficiency-prioritized droop control strategy of AC microgrid," *IEEE J. Emerg. Sel. Topics Power Electron.,* early access, 2019. Doi: 10.1109/JESTPE.2020.2967756.

[19] Y. Wang, D. Liu, P. Liu, F. Deng, D. Zhou, and Z. Chen, "Lifetime-oriented droop control strategy for AC islanded microgrids," *IEEE Trans. Ind. Appl*., vol. 55, no. 3, pp. 3252-3263, Feb. 2019.

[20] Y. Wang, X. Wang, Z. Chen, and F. Blaabjerg, "Distributed optimal control of reactive power and voltage in islanded microgrids," *IEEE Trans. Ind. Applicat.*, vol. 53, no.1, pp. 340-349, Feb. 2017.

[21] X. Hou, Y. Sun, H. Han, Z. Liu, W. Yuan, and M. Su. "A fully decentralized control of grid-connected cascaded inverters," *IEEE Trans. Sustainable Energy*, vol. 10, no.1 pp.315-317, Jan. 2019.

[22] T. V. Hoang and H.-H. Lee, "An adaptive virtual impedance control scheme to eliminate the reactive-power-sharing errors in an islanding meshed microgrid," *IEEE J. Emerg. Sel. Topics Power Electron.*, vol. 6, no. 2, pp. 966-976, Jun. 2018.

[23] P. Lin, T. Zhao, B. Wang, Y. Wang, and P. Wang, "A semi-consensus strategy toward multi-functional hybrid energy storage system in DC microgrids," *IEEE Trans. Energy Convers.*, early access, 2019. Doi: 10.1109/TEC.2019.2936120.

[24] W. Yuan, Y. Wang, D. Liu, F. Deng, and Z. Chen, "Robust droop control of AC microgrid against nonlinear characteristic of inductor," in *Proc. PEDG*, Jun 3-6, 2019. pp. 1-6.

[25] R. Lasseter, "Smart distribution: Coupled microgrids," *Proc. IEEE*, vol. 99, no. 6, pp. 1074-1082, Jun. 2011.

[26] Y. Wang, Z. Chen, X. Wang, Y. Tian, Y. Tan, and C. Yang, "An estimator-based distributed voltage predictive control strategy for AC islanded microgrids," *IEEE Trans. Power Electron.*, vol. 30, no. 7, pp. 3934-3951, July. 2015.

[27] W. Yuan, Y. Wang, X. Ge, X. Hou, and H. Han, "A unified distributed control strategy for hybrid cascaded-parallel microgrid," *IEEE Trans. Energy Convers.*, vol. 34, no. 4, pp. 2029-2040, Dec. 2019.

[28] M. C, Chandorkar, D. M. Divan, and R. Adapa, "Control of parallel connected inverters in standalone ac supply systems," *IEEE Trans. Ind. Appl.,* vol.29, no.1 pp.136-143, Jan.1993.

[29] D. Halliday, R. Resnick, and J. Walker, *Fundamentals of Physics, Chapters 28-31*, 10th ed. John Wiley & Sons, 2010.

[30] "Magnetics powder core catalog", 00K6527E026, *Magnetics datasheet*, 2014.

[31] "Magnetics powder core catalog", 00K160LE026, *Magnetics datasheet*, 2013.

[32] A. Isidori, *Nonlinear Control Systems*. New York: Springer-Verlag, 1995.

[33] J. M. Guerrero, L. G. Vicuña, J. Matas, M. Castilla, and J. Miret, "Output impedance design of parallel-connected UPS inverters with wireless load-sharing control," *IEEE Trans. Ind. Electron.*, vol. 52, no. 4, pp. 1126-1135, Aug. 2005.

[34] Y. Wang, X. Wang, F. Blaabjerg, and Z. Chen, "Harmonic instability assessment using state-space modeling and participation analysis in inverter-fed power system," *IEEE Trans. Ind. Electron.*, vol. 64, no. 1, pp. 806-816, Jan. 2017.

[35] E. A. A. Coelho, P. C. Cortizo, and P. F. D. Garcia, "Small-signal stability for parallel-connected inverters in stand-alone AC supply systems," *IEEE Trans. Ind. Appl*., vol. 38, no. 2, pp. 533-542, Mar. 2002.

[36] N. Pogaku, M. Prodanovic´, and T. C. Green, "Modeling, analysis and testing of autonomous operation of an inverter-based microgrid," *IEEE Trans. Power Electron.*, vol. 22, no. 2, pp. 613-625, Mar. 2007.

[37] Y. Wang, X. Wang, Z. Chen, and F. Blaabjerg, "Small-signal stability analysis of inverter-fed power systems using component connection method," *IEEE Trans. Smart Grid*, vol. 9, no. 5, pp. 5301-5310, Sep. 2018.

[38] Kundur, P., Neal J. Balu, and Mark G. Lauby. *Power System Stability and Control*, *Chapter 12*, New York: McGraw-Hill, 1994.

Wenbin Yuan received the B.Eng. degree from Xiangtan University, Xiangtan, China, in 2015, and M.Sc. degree from the School of Information Science and Engineering, Central South University, Changsha, China, in 2018.

Currently, he is working toward Ph.D. degree in the Department of Energy Technology, Aalborg University, Denmark.

His research interests include distributed power generation system, microgrid, as well as control technologies of power electronic-dominated power system.

Yanbo Wang (S'15-M'17-SM'19) received Ph.D. degree in the Department of Energy Technology, Aalborg University, Denmark, in 2017. Currently, he is with the Department of Energy Technology in Aalborg University as an Assistant Professor. From June to October of 2016, he was a visiting scholar in Power System Research Group of the Department of Electrical and Computer Engineering, University of Manitoba, Winnipeg, MB, Canada. His research interests include distributed power generation system, wind power system, microgrid, as well as operation and control technologies of power electronic-dominated power system.

Dr. Wang's paper on Distributed Power System received the First Prize Paper Award of the 6th International Conference of Smart Grid cosponsored by IEEE Industry Application Society in 2018. He received the Best Session Paper Award at the annual conference of the IEEE Industrial Electronics Society in 2015 in Japan.

Dong Liu (S'15-M'18-SM'19) received the B.Eng. and M.Sc. in electrical engineering from South China University of Technology, Guangzhou, China, in 2008 and 2011, and the Ph.D. degree in energy technology from the Department of Energy Technology, Aalborg University, Aalborg, Denmark, in 2018. Currently, he is with the Department of Energy Technology in Aalborg University as a Postdoctoral Researcher.

From 2011 to 2014, he was an R&D engineer in Emerson Network Power Co., Ltd., Shenzhen, China. From May, 2017 to November, 2017, he was a visiting scholar at Center for Power Electronics Systems (CPES), Virginia Tech, Blacksburg, VA, USA. His main research interests include the modeling and control of power electronics converters, high-efficiency power conversion systems, and power electronics applications in renewable energy power generations.

Fujin Deng (SM'19) received the B.Eng. degree in Electrical Engineering from China University of Mining and Technology, Jiangsu, China, in 2005, the M.Sc. degree in Electrical Engineering from Shanghai Jiao Tong University, Shanghai, China, in 2008, and the Ph.D. degree in Energy Technology from the Department of Energy Technology, Aalborg University, Aalborg, Denmark, in 2012.

He joined the Southeast University in 2017 as a Professor in the School of Electrical Engineering, Southeast University, Nanjing, China. From 2013 to 2015 and from 2015 to 2017, he was a Postdoctoral Researcher and an Assistant Professor, respectively, in the Department of Energy Technology, Aalborg University, Aalborg, Denmark. His main research interests include wind power generation, multilevel converters, high-voltage direct-current technology, DC grid and offshore wind farm-power systems dynamics.

Zhe Chen (M'95-SM'98-F'18) received the B.Eng. and M.Sc. degrees from Northeast China Institute of Electric Power Engineering, Jilin City, China, in 1982 and 1986, and the Ph.D. degree from University of Durham, U.K., in 1997.

Dr. Chen is a full Professor with the Department of Energy Technology, Aalborg University, Denmark. He is the leader of Wind Power System Research program at the Department of Energy Technology, Aalborg University and the Danish Principle Investigator for Wind Energy of Sino-Danish Centre for Education and Research. His research areas are power systems, power electronics and electric machines, and his main current research interests are wind energy and modern power systems. He has led many research projects and has more than 500 publications in his technical fields.